COMMUNICATION

Fabrication of Transparent Multilayer Circuits by Inkjet Printing

Jieke Jiang, Bin Bao, Mingzhu Li, Jiazhen Sun, Cong Zhang, Yang Li, Fengyu Li, Xi Yao, and Yanlin Song*

Printed electronics have attracted increasing attention in recent years as an alternative to conventional silicon-based technologies to realize a range of low-cost, large-area, and flexible functional devices such as conductive circuits,[1] organic thin-film transistors,[2] and photovoltaic devices.[3] Compared with various methods to assemble conductive materials into electronic devices, such as template-assisted assembly,[4] spin-coating,[5] lithographic patterning,[6] and so on,[7] inkjet printing offers a mask-free, cost-effective, and digital method to fabricate functional patterns in large scale. Specifically, by patterning conductive inks on plastic substrates, inkjet printing provides new opportunities for the manufacture of transparent and flexible electronics.[8] However, inkjet printing could only fabricate low-aspect ratio patterns sometimes with bulges or splashed boundaries due to the spreading phenomenon of the inkjet printed droplets.[9] The inevitably ink spreading critically determines the resolution[10] and morphology of printed patterns, thereby the integration degree and electrical stability of printed electronics.[11] Moreover, wide conductive lines caused by ink spreading would also reduce the transmittance of printed transparent electronics.[12] So far, various strategies have been developed to steer the ink spreading for achieving high-resolution inkjet printed patterns. One approach is to predefine physical and chemical patterns on a substrate that force the ink to remain in a preferred area on the substrate.[13] This method requires patterned surface treatments, which needs the use of masks and complex processing steps. In another approach, the contact angle of ink droplet is enlarged by modifying the substrate with a low surface energy coating, hence the resolution of resulted patterns is improved through the dynamically retreating of the three-phase contact line (TCL).[14] However, ink droplets printed on low surface energy substrate tend to form line bulges or even coalesce into a large droplet due to the unconstrained sliding of the TCL.[9b,15] Recently, Lewis et al. demonstrated an promising embedded 3D printing method to fabricate strain sensors by extruding a viscoelastic ink with strong shear thinning property into an elastomeric reservoir.[16] By embedding the cylindrical shape conductive cables into elastomer, the ink spreading could be obviously inhibited. However, the fabrication of embedded conductive line by inkjet printing still remains a challenge, as the coalesce of low-viscosity ink droplets to form straight lines in another liquid is quite difficult to control.[17]

Here, we demonstrate an efficient method to inkjet print highly integrated embedded conductive microcables inside elastomers, named as embedded inkjet printing (e-IJP). Despite the fact that the resolution of inkjet printing is limited to typically 20 μm due to the spreading of ink droplet on solid substrate,[10a] conductive silver lines with 1.6 μm width and 1.7 aspect ratio were fabricated using a 25 μm orifice nozzle. This is one of the highest conductive line resolution ever achieved by piezoelectric inkjet printing method without any pre-patterning of the substrate. The resolution is comparable to the electric-field-based super inkjet printing technology.[18] The key of this strategy is to inkjet print conductive ink into a crosslinkable viscous liquid substrate. Thus, the spreading of the ink droplets was inhibited due to the encapsulation of the ink by viscous substrate. As a result, embedded conductive microcables with high resolution and aspect ratio were successfully fabricated. This method could directly integrate conductive microcables into flexible substrate, which needs no additional encapsulation processes. Finally, a transparent and bendable film with three layers of embedded conductive circuits was fabricated. Benefited from the embedded structure, the electrical performance of the circuits was stable even after thousands times of bending cycles.

Spin-coated poly(dimethylsiloxane) (PDMS) precursor film was used as the viscous liquid substrate for inkjet printing conductive microcables. PDMS was used because its widely application in elastomeric electronics, such as electronic skins and transparent flexible electrode, due to its high transparency and excellent flexibility.[19] Besides, the high viscosity and low surface energy of liquid PDMS precursor have been utilized to fabricate microfluidic and other functional devices.[17a,20] Here, we demonstrate that the liquid PDMS precursor substrate could be used to inkjet print high-resolution embedded microcables. Silver nanoparticles (AgNPs) suspension was used as the conductive ink due to its high conductivity and widespread application in printed electronics.[21] A schematic illustration of this

Dr. J. Jiang, Dr. B. Bao, Dr. M. Li, C. Zhang,
Y. Li, Dr. F. Li, Prof. Y. Song
Key Laboratory of Green Printing
Institute of Chemistry
Chinese Academy of Sciences (ICCAS)
Beijing Engineering Research Center of Nanomaterials
for Green Printing Technology
Beijing National Laboratory for Molecular Sciences (BNLMS)
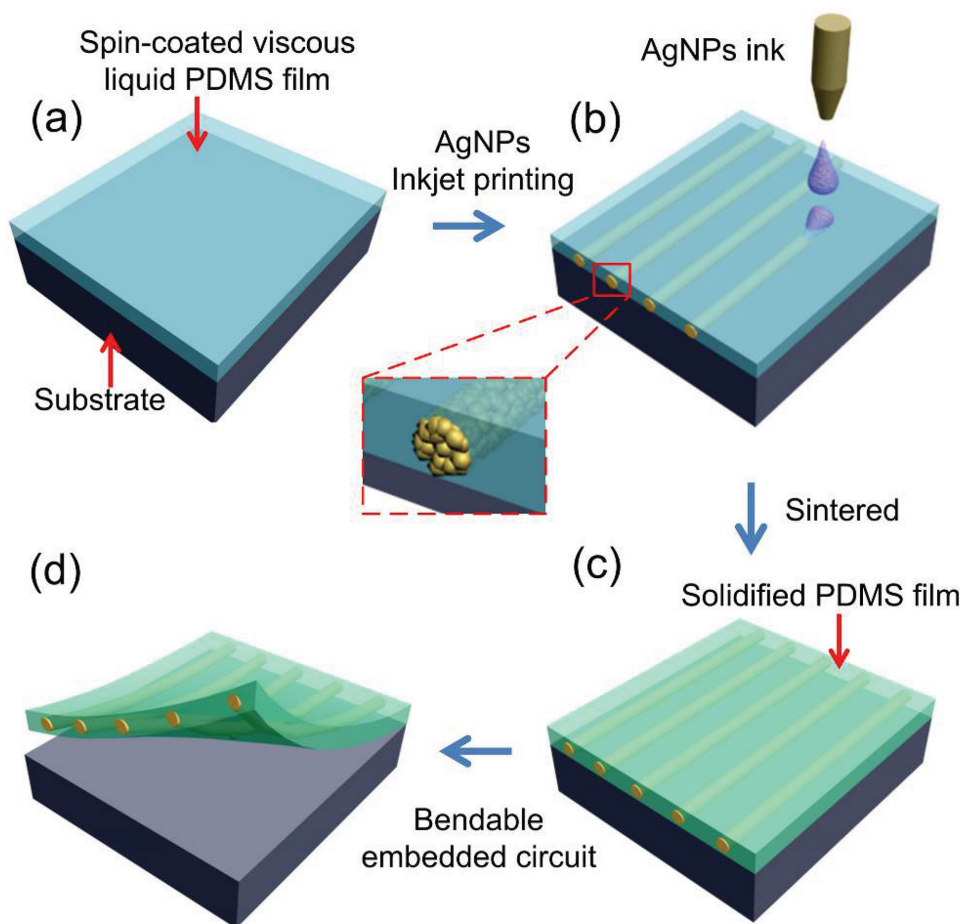Beijing 100190, P. R. China
E-mail: ylsong@iccas.ac.cn
Dr. J. Jiang, Dr. B. Bao, Y. Li
University of Chinese Academy of Sciences
Beijing 100049, P. R. China
Dr. J. Jiang, Prof. X. Yao
Department of Biological Sciences
City University of Hong Kong
Tat Chee Avene, Hong Kong
Dr. J. Sun
School of Chemistry and Environment
Beihang University
Beijing 100191, P. R. China

Scheme 1. Schematic illustration of inkjet-printed embedded silver microcables. a) Viscous liquid PDMS precursor was spin-coated on a cleaned PET substrate to form a viscous liquid substrate. b) AgNP ink was inkjet-printed on the liquid substrate. Inside the PDMS film, adjacent droplets coalesce forming embedded silver microcables. c) The AgNP cables were encapsulated by the PDMS film and were sintered after the printing process. d) The PDMS film with embedded silver cables could be peeled off from the PET substrate.

method is presented in **Scheme 1**. The liquid PDMS precursor was spin coated on a cleaned polyethylene terephthalate (PET) film, forming a layer of viscous liquid substrate with thickness of ≈20 μm (Scheme 1a). Owing to the viscosity of the PDMS precursor and the impact force imposed by the ink droplets, the inkjet printed AgNPs would fully sink into the PDMS film. The interaction between ink droplet and the liquid viscous substrate could be well controlled by adjusting the rheological property of the substrate and the concentration of AgNP inks. With optimized rheological property and ink concentration, the printed droplets coalesced into microcables inside the PDMS matrix (Scheme 1b). Subsequently, the PDMS film with embedded AgNP microcables was sintered at 150 °C for 2 h to enhance its conductance (Scheme 1c). Finally, the PDMS film with printed silver cables could be peeled off from the PET substrate, forming an embedded circuit within a transparent film (Scheme 1d).

Uniform AgNPs with diameters in the range of 40–60 nm (Figure S1, Supporting Information) were synthesized using polyvinylpyrrolidone (PVP) as the protectant[22] and dissolved in a mixture of ethanol and water to formulate the AgNP ink. To print narrow lines without bulges on solid surfaces, the match

of surface energy between the substrate and the printing ink is necessary. To fabricate high-resolution embedded silver lines by the e-IJP technique, the match of surface tension is also critical. First, pure water was used as the ink solvent. It was found that only discontinuous ink droplets were obtained due to the much larger surface tension of the inks (about 72 mN m^{-1}) compared to that of the liquid PDMS substrate (about 21.6 mN m^{-1}), as shown in Figure S2a (Supporting Information). Then, pure ethanol was used as the solvent to match the surface tension of AgNP ink with the liquid PDMS substrate. However, the fast evaporation of ethanol may lead to clogging of the printing nozzles, resulting in the formation of discontinuous lines (Figure S2b, Supporting Information). Finally, solvent with volume ratio between water and ethanol as 1:9 was optimized to achieve a balance between lowering the surface tension of the ink and preventing the clogging of the nozzle, as shown in Figure S2c (Supporting Information). When the immiscible AgNP ink droplet was inkjet printed on the viscous substrate, the droplet would penetrate into the PDMS precursor matrix forming embedded cable structures. **Figure 1**a is the optical image of the large scale and uniform printed silver cables. By dissolving the uncrosslinked substrate with cyclohexane, the
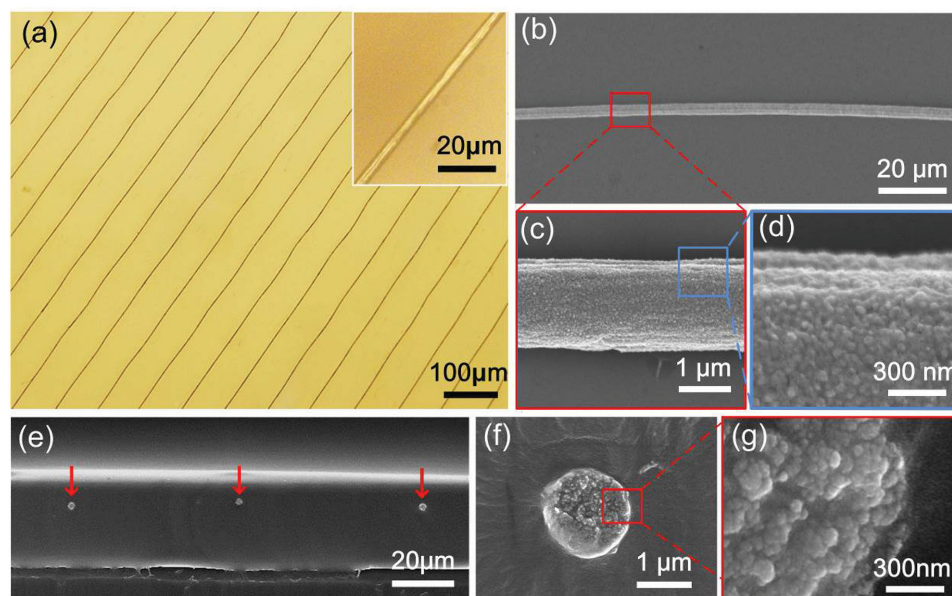
Figure 1. Large-scale embedded silver microcables fabricated by e-IJP. a) Optical observation of large-scale embedded silver cables. The distance between two adjacent lines is set as 60 μm. Insert is the magnification of a single embedded silver cable. b–d) SEM characterization from the front view of the silver cable before sintering. The microcable was obtained by dissolving the PDMS precursor by cyclohexane. The magnified SEM image clearly shows that the silver cable is composed of closely assembled AgNPs. e) SEM image of the cross section of as-prepared three adjacent silver cables. f) Magnified SEM image of the cross section of an individual silver cable. The height, width, and aspect ratio of the embedded silver cable are 1.6 μm, 1.6 μm, and 1.0, respectively. g) Magnified SEM image of embedded silver cable cross section, showing those AgNPs have been sintered into larger grain size after being heated at 150 °C for 2 h.

embedded silver cables was characterized by scanning electron microscope (SEM) (see Figure 1b–d). The single-line resolution of the as printed silver cable was ≈1.6 μm and the silver cable was composed of closely assembled AgNPs. Figure 1e–g exhibit the SEM observations of the cross sections of embedded silver microcables. Different from previously reported low aspect-ratio flat silver tracks printed on solid substrates,[23] this e-IJP method could directly fabricate silver lines with circular cross section, which would dramatically advance the resolution of printed conductive line. Figure 1g demonstrates that those AgNPs are sintered to form larger grain sizes after being heated for 2 h at 150 °C. Induced by the suppression and encapsulation of the viscous liquid substrate, the aspect ratio of the embedded cylindrical architecture was comparable or even higher than the reported direct ink writing results.[9a]

During the droplet sinking process (as simulated in Figure S3, Supporting Information), the ink droplet would penetrated into the viscous substrate within 4 s as it was deposited due to its impact force. Then, the ink droplet would form spherical shape to minimize its surface energy. Supported by the viscous PDMS precursor, the ink droplet was sealed into the substrate closely to the surface until it was sintered. After thermal crosslinking of PDMS, there is no hollow space formed around the silver microcables. The reason is attributed to the fast evaporation of the ink solvent and the continuous compression of the liquid PDMS. The ink solvent is a mixture of 90% ethanol and 10% water in volume, which evaporated much faster than water. The ink droplet is about 10 pL. Thus, the solvent of the ink droplets was evaporated during the ink embedding process before the solidification of the liquid

PDMS substrates. With the evaporation of the solvents, the liquid PDMS compresses the silver lines continuously before thermal curing. To make clear the influence of PDMS with or without curing on the shape of Ag lines, we gently touched the Ag lines using the tip of a tweezers when the substrate is still in the liquid state (see Movie S1, Supporting Information). It showed that the Ag line had already been rigid before the thermal curing process. The following sintering process made the AgNPs melt and improved the bending durability and conductivity of the printed Ag line.

The wrapping ability of the PDMS film was crucial for the fabrication of encapsulated silver microcables, which was demonstrated by printing conductive lines on PDMS substrate with different procured time (Figure S4–S6, Supporting Information). Besides, the AgNP ink concentration was another crucial factor for the fabrication of embedded silver cables. The diameter of the microcable increased as the ink concentration improved from 3.0 to 7.0 wt%, while 1.0 wt% ink forming discontinuous silver cables and 10% ink forming ellipse-shape cross-section cables, as exhibited in **Figure 2**a,b. Since the Rayleigh–Taylor instability[24] exists inside the inkjet printed ink-line, the AgNPs tended to assemble into segments when using diluted AgNP ink. As a result, the embedded silver microcable broke into discontinuous fragments due to the low AgNPs content of 1.0 wt% ink. When the ink concentration increased to 3.0 wt%, the silver line discontinuity was suppressed due to the sufficiency of AgNP building blocks. The statistical size of 50 silver cables cross sections shows the width and height both ranged from 1.3 to 1.8 μm (see Figure S7, Supporting Information), which demonstrates the high reliability
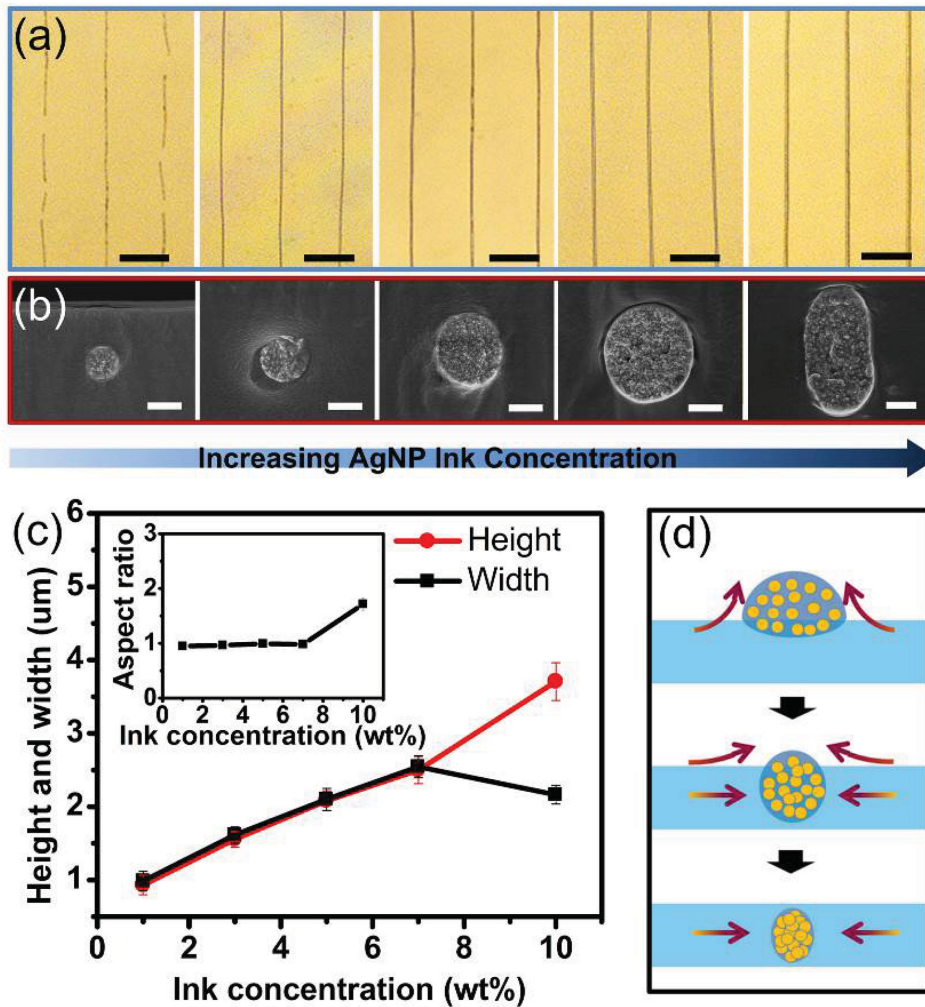
Figure 2. The morphology of embedded silver cables controlled by adjusting the AgNP ink concentration. a) Optical images of silver microcables inkjet printed with (from left to right) 1.0, 3.0, 5.0, 7.0, and 10.0 wt% AgNP ink, respectively. Only the 1.0 wt% AgNP ink printed silver cables break into segments. The scale bar is 50 μm. b) SEM images of silver cable cross sections corresponding in (a). The scale bar is 1 μm. c) Statistical distribution of the height and width of embedded silver cables with increasing AgNP ink concentration. Inset is the aspect ratios (height/width) of embedded microcables in corresponding to the increase of AgNP ink concentrations. Error bars represent standard deviation from 15 samples. d) Schematic illustration of the encapsulation process.

of this e-IJP method. When the ink concentration increased from 3.0 to 7.0 wt%, the diameters of silver cables varied from 1.6 to 2.5 μm. However, as the ink concentration increased to 10.0 wt%, the cross section of printed silver cable altered from round-shape to ellipse-shape, which was stretched in the vertical direction. As a result, there was a sharp decline in the statistics data of line width as the AgNPs ink concentration increased to 10.0 wt% (see Figure 2c). However, when the ink concentration rose to above 10.0 wt%, the nozzle was clogged severely. The height of 10.0 wt% silver line reached 3.7 μm while the width kept 2.0 μm, which was consistent with the results produced by repeated experiments (Figure S8, Supporting Information). As illustrated in Figure 2d, ink droplet was squeezed by surrounded liquid PDMS precursor during the ink droplet impact into the substrate, indicating greater horizontal squeezing force was loaded when the 10.0 wt% ink droplet occupied a larger volume and imposed a higher impact force. As the cross

section of silver line varied from circle to ellipse, the average silver cable aspect ratio improved from 1.0 to 1.7, which would be promising in fabricating highly transparent conductive film and printing extremely integrated circuit board.

Currently, commercially available printed circuit board (PCB) uses two layers of adhesives to encapsulate conductive copper tracks inside two layers of polyimide.[25] While the thickness of single-layer PCB is above 130 μm, the thickness of multilayers PCB is much higher as more layers of adhesives were used. This e-IJP method could integrate three layers of circuits within a 100 μm thick transparent film. The multilayer circuits were printed with a layer-by-layer manner, in which the subsequent PDMS layer was spin coated after the former layer circuit was printed and solidified (as shown in Figure S9 in Supporting Information). The optical microscope images of one layer, two layers, and three layers circuits were shown in **Figure 3**a–c, respectively. To distinguish specific layers, trace
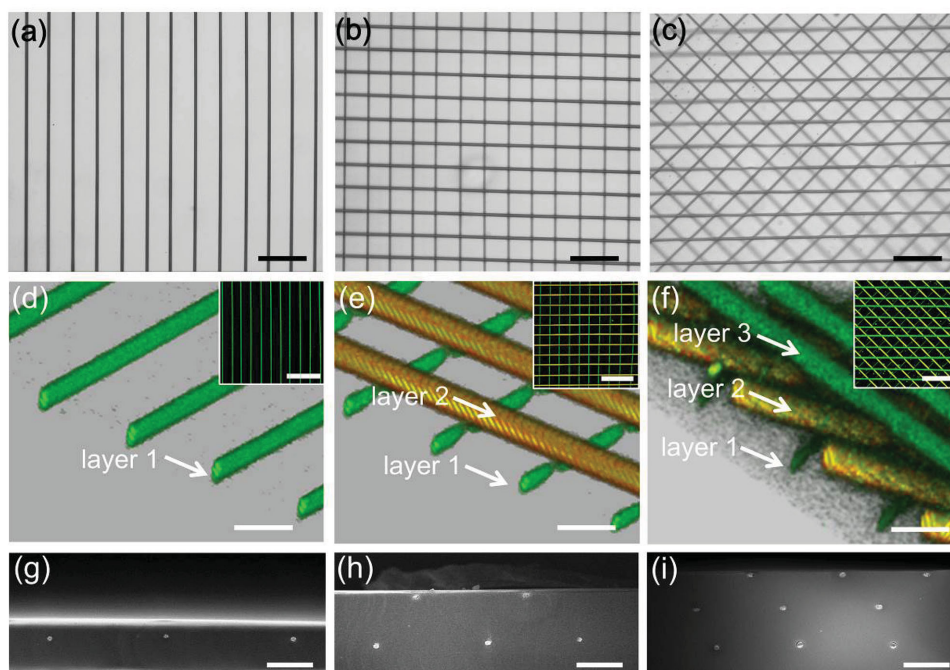
COMMUNICATION

Figure 3. The morphology of embedded multilayer circuits fabricated by e-IJP in a layer-by-layer manner. a–c) Optical microscope images of different layers embedded circuits fabricated by e-IJP after the former layer of circuit was solidified. The scale bar is 100 μm. d–f) 3D confocal laser scanning microscope observation of single, double, and three layers circuits labeled by green and yellow fluorescent colors alternatively. The scale bar is 100 μm. Insets are fluorescent images of multilayer circuits in full view. The scale bar is 200 μm. g–i) SEM images of single, double, and three layer circuits cross section, respectively, indicating the layered structure of embedded silver cables. The scale bar is 50 μm.

amount of fluorescent agent uranine and rhodamine B were added, respectively, into the AgNPs ink to form two kinds of fluorescent labeled inks. The two labeled inks were used alternatively to fabricate the multilayer circuits. As a result, silver cables with green and yellow colors embedded inside the PDMS film could be visualized in 3D through the confocal laser scanning microscope observation, as shown in Figure 3d–f. The 3D fluorescent images indicate the cylindrical shape of single embedded silver cable and the multilayer structure of the integrated circuits. The SEM images of the cross sections of one layer, two layers, and three layers embedded circuits are shown in Figure 3g–i, respectively. The thickness of the embedded circuit increased from ≈30 to ≈100 μm when the circuits increased from one layer to three layers. The 30 μm thick PDMS between the adjacent circuit layers works as effective insulation.

Moreover, the embedded circuit exhibits high transparency and stable conductivity. **Figure 4**a shows a transparent conductive film with three layers embedded silver circuits fitting closely together with the hand, indicating its high conformability with human skin. The amplified digital photograph of the highly transparent embedded circuits was shown in Figure 4b. As a comparison, we inkjet printed AgNP ink on a commercially PET film resulting ≈100 μm width silver tracks, which make the film non-transparent (Figure S10, Supporting Information). Figure 4c are the UV–vis spectroscopies of printed 60 μm spacing silver cables into PDMS film with different layers. The transmittance of single-layer embedded circuit kept at 95% and three layers embedded circuits still had the transparency of 85% among 400 to 900 nm wavelength. The electrical performance of the embedded circuits was tested by

coating conductive paste on two opposite cross sections of the PDMS film (Figure S11, Supporting Information). The resistivity of embedded cable was measured as 1.67×10^{-6} Ω m (the average of five times independent measurements) by testing the conductivity of single embedded cable. Figure 4d presents the change in resistance as a function of bending radius. As the embedded circuit film deformed from flat to 4 mm bending radius, the circuit remained conductive (also see Figure S12, Supporting Information), with only a little resistance change between 360 ± 15 Ω. The stable conductivity of the circuits was mainly caused by the protection of the encapsulation structure. The I–V behavior of the embedded circuit under different bending radii was performed, shown in Figure 4e. Remarkably, under different bending statuses, the embedded circuits exhibited similar linear increase of the current when the sweeping voltage increased, indicating well ohm contact among AgNPs. Notably, there was no apparent resistance increase after the PDMS film was bended 3000 times (see Figure 4f). Encapsulated by PDMS film, the silver cables were protected from forming fractures. As a comparison, silver tracks inkjet printed on PET surface using the same AgNPs ink were tested as the control sample. The resistance of PET film increased quickly and cannot recover when the PET was flattened out.

In conclusion, embedded silver microcables were fabricated by inkjet printing AgNP ink into viscous liquid PDMS precursor film. By controlling the spreading of ink droplet and the rheological property of liquid substrate, the resolution of a single silver line reached 1.6 μm. The inhibition of ink spreading made the embedded circuit both highly integrated and transparent. With a layer-by-layer manner, the method was
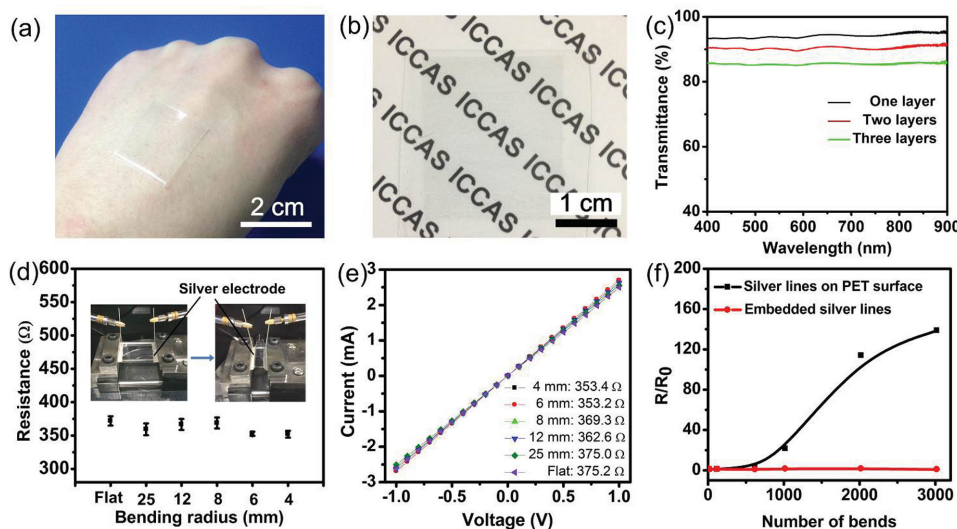
Figure 4. Optical and electrical characterization of the transparent embedded circuit. a) Digital photograph of a three layers embedded circuits shows well conformability of the circuits to human skin. b) Amplified digital photograph of the highly transparent three layers circuits. c) Transmittance spectra of the printed 60 μm spacing silver lines in PDMS film with different printing layers. The transmittance of single-layer embedded circuit kept at ≈95% and three layers embedded circuits still had the transparency of above 85% among 400 to 900 nm wavelength. d) Relationship between the resistance of embedded circuit and the bending radius within a single bending cycle. The conductivity remained stable as the bending radius was decreased. e) Current–voltage curve of the embedded circuit containing 50 parallel silver microcables under different bending radii. The embedded circuits exhibited similar linear increase of current when the sweeping voltage increased from −1.0 to 1.0 V under all bending radii. f) Comparison of resistance increment versus bending times of embedded silver microcables and silver lines inkjet printed on PET film. The resistance of conductive tracks on PET film increased dramatically with increasing bending times while that of the embedded microcables remained stable. The conductivity was measured when the films were flattened.

employed to print transparent multilayer microcircuits. As the silver cables were encapsulated by PDMS matrix, the embedded circuits could be bended reversely without apparent resistance increase. The simple inkjet printing technique to fabricate embedded conductive microcables will provide a promising avenue for highly integrated circuit board and highly transparent devices.

Experimental Section

Preparation of Viscous Liquid Substrates: Commercial transparent plastic PET films (75 μm thick, Shenzhen HonghaoTechnology Co., Ltd. China) were rinsed by deionized water and ethanol before dried in air and cut into dimensions of ≈3 cm × 3 cm. PDMS (Sylgard 184, Dow Corning) base was mixed with curing agent in the proportion of 10:1 by weight to prepare PDMS precursor. The precursor was put into a centrifuge to remove air bubbles (2000 rpm, 5 min) before spin-coated onto the PET substrates (first 800 rpm for 10 s, then 3000 rpm for 30 s). Subsequently, the PDMS precursor was precured in an 80 °C oven for a given time, resulting the printing substrate.

Preparation of AgNP Conductive Inks: AgNPs were prepared according to previous reports.[22,26] In a typical synthesis of AgNPs, 6.0 g PVP ($M_w = 1 \times 10^4$ g mol^{-1} Sigma–Aldrich) was dissolved in 50 mL ethylene glycol, and 1.2 g AgNO$_3$ was added into the above solution. The suspension was then stirred at 60 °C until AgNO$_3$ was completely dissolved. Then, the system was heated up to 120 °C and remained for 1 h at this temperature to allow the reaction to complete. After the mixture was cooled to room temperature, the AgNPs were easily separated from the system as an amount mixture of acetone and ethanol (2/1, w/w) were added. After drying under vacuum at 60 °C for 30 min, the obtained bright-yellow powders were dispersed in a mixture of ethanol (90.0 wt%) and water (10.0 wt%). Trace amount of uranine

(J&K Scientific Ltd.) and rhodamine B (96%, J&K Scientific Ltd.) was added to formulate 10 μg mL^{-1} green and yellow fluorescent labeled ink.

Fabrication of Embedded Silver Microcables by e-IJP: The conductive ink was treated ultrasonically and filtered through a 1.5 μm pore size cellulose ester filter to avoid nozzle clogging before it was injected into an inkjet cartridge. The concentration of the ink ranged from 1.0 to 10.0 wt%. The printing of the conductive ink was performed by a Dimatix Fujifilm DMP-2800 printer with 10 pl Dimatix materials cartridge, which was controlled with the Dimatix Drop Manager software. Only one nozzle was used during the printing process. The printing frequency was set as 5.0 kHz and a customized waveform was utilized, which had a maximum of 30 V and a pulse width of 8.5 μs. The second and third layer circuits were printed in the same way, after the former layer circuit was printed and solidified at 150 °C for 5 min. After all the layers finished, the sample was heated at 150 °C for 2 h to make the PDMS layer solidified and the AgNPs sintered as well as the protectant decomposed.

Characterization: The structures of embedded silver microcables were investigated by a scanning electron microscopy (SEM, JEOL, JSM-7500F, Japan) at an accelerating voltage of 3.0 kV. The optical images of PDMS film after inkjet printing AgNP ink were acquired by two optical microscopes (Vision Engineering Co., UK, and Nikon Co., Japan), both were coupled to a CCD camera. The transmittance of the conductive film was measured using a UV–vis spectrophotometer (Shimadzu, UV 2600, Japan). Static contact angles were measured on a Dataphysics (Germany) OCA20 contact-angle system at ambient temperature. The 3D confocal laser scanning microscope image of the PDMS film with embedded silver lines was acquired by confocal laser scanning biological microscope (Olympus, FV1000-IX81, Japan).

Electrical Measurement of the Embedded Silver Microcables: Conductive silver adhesive (NT-ST60, Nano Top Co., Ltd. China) was pasted on the cross sections of the embedded silver microcables by cutting off two ends of the PDMS film perpendicularly to the embedded silver lines. The two electrodes were contacted with two platinum probes to measure the resistance on the Keithley 4200-SCS semiconductor analyzer. The cross-sectional area was measured according to the SEM images. The

**ADVANCED
MATERIALS**
www.advmat.de

**Materials
Views**
www.MaterialsViews.com

COMMUNICATION

resistivity ρ was calculated from the resistance R, the length L, the cross-sectional area A of a single conductive cable, using $\rho = RA/L$.

Supporting Information

Supporting Information is available from the Wiley Online Library or from the author.

Acknowledgements

[1] a) S. B. Walker, J. A. Lewis, *J. Am. Chem. Soc.* **2012**, *134*, 1419; b) J. Perelaer, R. Abbel, S. Wünscher, R. Jani, T. van Lammeren, U. S. Schubert, *Adv. Mater.* **2012**, *24*, 2620; c) Z. Zhang, X. Zhang, Z. Xin, M. Deng, Y. Wen, Y. Song, *Adv. Mater.* **2013**, *25*, 6714.

[2] a) H. Sirringhaus, T. Kawase, R. H. Friend, T. Shimoda, M. Inbasekaran, W. Wu, E. P. Woo, *Science* **2000**, *290*, 2123; b) M. L. Hammock, O. Knopfmacher, T. N. Ng, J. B. H. Tok, Z. A. Bao, *Adv. Mater.* **2014**, *26*, 6138; c) H. Minemawari, T. Yamada, H. Matsui, J. Tsutsumi, S. Haas, R. Chiba, R. Kumai, T. Hasegawa, *Nature* **2011**, *475*, 364; d) H. L. Wang, B. Hsieh, G. Jimenez-Oses, P. Liu, C. J. Tassone, Y. Diao, T. Lei, K. N. Houk, Z. N. Bao, *Small* **2015**, *11*, 126; e) Y. Noguchi, T. Sekitani, T. Yokota, T. Someya, *Appl. Phys. Lett.* **2008**, *93*, 043303; f) T. Sekitani, K. Zaitsu, Y. Noguchi, K. Ishibe, M. Takamiya, T. Sakurai, T. Someya, *IEEE Trans. Electron Devices* **2009**, *56*, 1027.

[3] a) C. N. Hoth, S. A. Choulis, P. Schilinsky, C. J. Brabec, *Adv. Mater.* **2007**, *19*, 3973; b) D. Angmo, T. T. Larsen-Olsen, M. Jorgensen, R. R. Sondergaard, F. C. Krebs, *Adv. Energy Mater.* **2013**, *3*, 172; c) Z. H. Wei, H. N. Chen, K. Y. Yan, S. H. Yang, *Angew. Chem. Int. Ed.* **2014**, *53*, 13239.

[4] a) S. Y. Yin, Y. Goldovsky, M. Herzberg, L. Liu, H. Sun, Y. Y. Zhang, F. B. Meng, X. B. Cao, D. D. Sun, H. Y. Chen, A. Kushmaro, X. D. Chen, *Adv. Funct. Mater.* **2013**, *23*, 2972; b) B. Su, C. Zhang, S. R. Chen, X. Y. Zhang, L. F. Chen, Y. C. Wu, Y. W. Nie, X. N. Kan, Y. L. Song, L. Jiang, *Adv. Mater.* **2014**, *26*, 2501; c) Z. Y. Zeng, X. Huang, Z. Y. Yin, H. Li, Y. Chen, H. Li, Q. Zhang, J. Ma, F. Boey, H. Zhang, *Adv. Mater.* **2012**, *24*, 4138.

[5] Z. Y. Yin, S. Y. Sun, T. Salim, S. X. Wu, X. A. Huang, Q. Y. He, Y. M. Lam, H. Zhang, *ACS Nano* **2010**, *4*, 5263.

[6] H. Lim, J. H. Noh, D. G. Choi, W. D. Kim, R. Maboudian, *J. Nanosci. Nanotechnol.* **2010**, *10*, 5020.

[7] a) J. Park, Y. Lee, J. Hong, Y. Lee, M. Ha, Y. Jung, H. Lim, S. Y. Kim, H. Ko, *ACS Nano* **2014**, *8*, 12020; b) Y. Kim, J. Zhu, B. Yeom, M. Di Prima, X. L. Su, J. G. Kim, S. J. Yoo, C. Uher, N. A. Kotov, *Nature* **2013**, *500*, 59.

[8] a) J. Lee, D. H. Kim, J. Y. Kim, B. Yoo, J. W. Chung, J. I. Park, B. L. Lee, J. Y. Jung, J. S. Park, B. Koo, S. Im, J. W. Kim, B. Song, M. H. Jung, J. E. Jang, Y. W. Jin, S. Y. Lee, *Adv. Mater.* **2013**, *25*, 5886; b) J. W. Wu, R. D. Wang, H. X. Yu, G. J. Li, K. X. Xu, N. C. Tien, R. C. Roberts, D. C. Li, *Lab Chip* **2015**, *15*, 690; c) Z. Y. Lu, M. Layani, X. X. Zhao, L. P. Tan, T. Sun, S. F. Fan, Q. Y. Yan, S. Magdassi, H. H. Hng, *Small* **2014**, *10*, 3551.

[9] a) B. Y. Ahn, E. B. Duoss, M. J. Motala, X. Guo, S. I. Park, Y. Xiong, J. Yoon, R. G. Nuzzo, J. A. Rogers, J. A. Lewis, *Science* **2009**, *323*, 1590; b) M. Liu, J. Wang, M. He, L. Wang, F. Li, L. Jiang, Y. Song, *ACS Appl. Mater. Interfaces* **2014**, *6*, 13344; c) C. Kim, M. Nogi, K. Suganuma, Y. Yamato, *ACS Appl. Mater. Interfaces* **2012**, *4*, 2168.

[10] a) J. Z. Wang, Z. H. Zheng, H. W. Li, W. T. S. Huck, H. Sirringhaus, *Nat. Mater.* **2004**, *3*, 171; b) Z. N. Bao, *Nat. Mater.* **2004**, *3*, 137.

[11] a) B. K. Kjellander, W. T. Smaal, J. E. Anthony, G. H. Gelinck, *Adv. Mater.* **2010**, *22*, 4612; b) B. Derby, *Annu. Rev. Mater. Res.* **2010**, *40*, 395.

[12] H. Lu, J. Lin, N. Wu, S. H. Nie, Q. Luo, C. Q. Ma, Z. Cui, *Appl. Phys. Lett.* **2015**, *106*, 4.

[13] a) E. Menard, M. A. Meitl, Y. Sun, J.-U. Park, D. J.-L. Shir, Y.-S. Nam, S. Jeon, J. A. Rogers, *Chem. Rev.* **2007**, *107*, 1117; b) S. K. Park, D. A. Mourey, S. Subramanian, J. E. Anthony, T. N. Jackson, *Adv. Mater.* **2008**, *20*, 4145.

[14] a) M. Kuang, J. Wang, B. Bao, F. Li, L. Wang, L. Jiang, Y. Song, *Adv. Opt. Mater.* **2013**, *2*, 34; b) J. Lessing, A. C. Glavan, S. B. Walker, C. Keplinger, J. A. Lewis, G. M. Whitesides, *Adv. Mater.* **2014**, *26*, 4677.

[15] T. H. J. van Osch, J. Perelaer, A. W. M. de Laat, U. S. Schubert, *Adv. Mater.* **2008**, *20*, 343.

[16] J. T. Muth, D. M. Vogt, R. L. Truby, Y. Mengüç, D. B. Kolesky, R. J. Wood, J. A. Lewis, *Adv. Mater.* **2014**, *26*, 6307.

[17] a) Y. Z. Guo, L. H. Li, F. Y. Li, H. H. Zhou, Y. L. Song, *Lab Chip* **2015**, *15*, 1759; b) A. S. Utada, A. Fernandez-Nieves, J. M. Gordillo, D. A. Weitz, *Phys. Rev. Lett.* **2008**, *100*, 4.

[18] a) T. Yokota, T. Sekitani, Y. Kato, K. Kuribara, U. Zschieschang, H. Klauk, T. Yamamoto, K. Takimiya, M. Kuwabara, M. Ikeda, T. Someya, *MRS Commun.* **2011**, *1*, 3; b) T. Sekitani, Y. Noguchi, U. Zschieschang, H. Klauk, T. Someya, *Proc. Natl. Acad. Sci. USA* **2008**, *105*, 4976.

[19] C. Wang, D. Hwang, Z. Yu, K. Takei, J. Park, T. Chen, B. Ma, A. Javey, *Nat. Mater.* **2013**, *12*, 899.

[20] B. Bao, J. Jiang, F. Li, P. Zhang, S. Chen, Q. Yang, S. Wang, B. Su, L. Jiang, Y. Song, *Adv. Funct. Mater.* **2015**, *25*, 3286.

[21] M. Park, J. Im, M. Shin, Y. Min, J. Park, H. Cho, S. Park, M.-B. Shim, S. Jeon, D.-Y. Chung, J. Bae, J. Park, U. Jeong, K. Kim, *Nat. Nanotechnol.* **2012**, *7*, 803.

[22] P. Y. Silvert, R. Herrera-Urbina, N. Duvauchelle, V. Vijayakrishnan, K. T. Elhsissen, *J. Mater. Chem.* **1996**, *6*, 573.

[23] J. Perelaer, A. W. M. de laat, C. E. Hendriks, U. S. Schubert, *J. Mater. Chem.* **2008**, *18*, 3209.

[24] T. R. Powers, R. E. Goldstein, *Phys. Rev. Lett.* **1997**, *78*, 2555.

[25] A. C. Siegel, S. T. Phillips, M. D. Dickey, N. S. Lu, Z. G. Suo, G. M. Whitesides, *Adv. Funct. Mater.* **2010**, *20*, 28.

[26] Z. L. Zhang, X. Y. Zhang, Z. Q. Xin, M. M. Deng, Y. Q. Wen, Y. L. Song, *Nanotechnology* **2011**, *22*, 425601.